JOURNAL OF SOLID STATE CHEMISTRY **132,** 361–371 (1997)
ARTICLE NO. SC977475

Structure of $Ag_2Ce(H_2O)(NO_3)_5$ and Its Thermal Decomposition Studied by Temperature-Dependent X-Ray Powder Diffraction

N. Audebrand, J. P. Auffrédic, and D. Louër

Laboratoire de Chimie du Solide et Inorganique Moléculaire (UMR 6511, CNRS), Groupe de Cristallochimie, Université de Rennes 1, Avenue du Général Leclerc, 35042 Rennes cedex, France

Received February 17, 1997; in revised form May 6, 1997; accepted May 13, 1997

The structure of $Ag_2Ce(H_2O)(NO_3)_5$ was determined from single-crystal diffraction. The symmetry is monoclinic (space group $P2/c$): $a = 21.472(5)$, $b = 8.027(1)$, $c = 15.413(3)$ Å, $\beta = 90.45(2)^\circ$, $V = 2656.2(7)$ Å, $Z = 8$. The structure consists of infinite chains of Ce icosahedra linked by nitrate groups and running along [100]. The Ag atoms and water molecules are located between these chains. Eightfold and ninefold coordinated Ag polyhedra share common vertices giving infinite chains in the three directions. Temperature-dependent X-ray powder diffraction, combined with TGA and DSC, has allowed us to completely describe the thermal decomposition process. Depending on the atmosphere, the dehydration of the precursor yields $Ag_2Ce(NO_3)_5$ or a mixture of $Ag_3Ce_2(NO_3)_9$ and $Ag_6Ce(NO_3)_9$. $Ag_2Ce(NO_3)_5$ is stable under vacuum in a narrow temperature range and transforms into the two previous phases. Crystalline and liquid $AgNO_3$ are also observed. The reaction scheme in nitrogen and vacuum is precisely described. The final product is a mixture of nanocrystalline CeO_2 and large crystals of metallic Ag. The structural relationships between the anhydrous phase and the precursor are discussed.

INTRODUCTION

The crystal structure and thermal behavior of various nitrato complexes with the general formulas $M^I_2Ce^{IV}(NO_3)_6$ (M^I = alkaline or ammonium ion) (1–4) and $M^I_2Ce^{III}(NO_3)_5 \cdot nH_2O$ (5–7) have been reported in recent years. It has been shown that the decomposition scheme of these phases is complex and depends on the environmental atmosphere and the microstructural properties of the precursor. By means of temperature-dependent X-ray diffraction (TDXD) some unexpected features were pointed out, e.g., the double valence change of Ce during the decomposition of the ceric compounds (2–4) and the formation of amorphous rubidium nitrate during the decomposition of rubidium cerous nitrates $Rb_3Ce_2(NO_3)_9$ (3) and $Rb_2Ce(NO_3)_5 \cdot 4H_2O$ (6). At high temperature, the end decomposition product of these mixed cerium III and IV phases is pure nanocrystalline CeO_2, a consequence of the decomposition of the intermediate single nitrates. Then, it is of interest to know if similar features can be observed when the alkaline metal, or ammonium, is substituted by another monovalent cation such as silver. However, in the course of the investigation of the system $AgNO_3$–CeO_2–HNO_3–H_2O, attempts to synthesize a ceric silver nitrato complex were unsuccessful due to the reduction of ceric ions into cerous ions, probably catalyzed by silver cations, but cerous silver nitrate $Ag_2Ce(H_2O)(NO_3)_5$ was always obtained. The present paper deals with the synthesis, structure determination, and thermal behavior of this new compound.

EXPERIMENTAL

Material Preparation

The new compound was obtained from evaporation of a solution of reactive ceria (8) and silver nitrate in concentrated nitric acid. Another convenient method of synthesis was from the dissolution in concentrated nitric acid (Merck) at 150°C of analytical grade $Ce(NO_3)_3 \cdot 6H_2O$ and $AgNO_3$ (Prolabo) taken in the molar ratio 1:2. The solution was evaporated at 65°C until colorless rod-like crystals were formed. The crystals are hygroscopic. The structure determination described in this paper, as well as the thermogravimetry analysis, have shown that the chemical formula is $Ag_2Ce(H_2O)(NO_3)_5$. For the thermal study, the crystals were ground in cyclohexane using a micronizing mill from McCrone Research Associated, Ltd. An average particle size of 20 μm was estimated from optical microscopy measurements.

X-Ray Diffraction

X-ray powder diffraction data were collected by means of a Siemens D500 diffractometer equipped with an incident-beam monochromator (Cu$K\alpha_1$ radiation). To prevent the hydration of the hygroscopic compounds, the samples were kept in a nitrogen atmosphere by using a tight sample holder. In addition, *in situ* powder diffraction data were

0022-4596/97 $25.00

obtained from a Siemens diffractometer equipped with a diffracted-beam monochromator ($CuK\alpha_{1,2}$ radiation) and a high-temperature attachment. Patterns were scanned with a step length of 0.02°(2θ). The peak positions were extracted by the pattern decomposition technique using the fitting program PROFILE from Socabim, available in the software package DIFFRAC-AT supplied by Siemens. Indexing of the powder patterns was performed with the program DICVOL91 (9).

Temperature-dependent X-ray powder diffraction (TDXD) was carried out with a diffractometer equipped with an INEL (CPS120) curved position detector. The detector was used in a semifocusing geometry by reflection ($CuK\alpha_1$ radiation) described elsewhere (10). The sample is stationary and located at the center of the goniometer. An angle of 6° was selected between the incident beam and the surface of the sample. The specimens were located in a monitored high-temperature device (Rigaku). To ensure satisfactory counting statistics, a counting time of 2000 or 2500 s per pattern was selected.

For the single-crystal diffraction study, a crystal was mounted on an Enraf-Nonius CAD-4 diffractometer equipped with a graphite monochromator ($MoK\alpha$ radiation). The crystal used for the structure analysis was introduced in a capillary containing dry oil to prevent its decomposition. Additionally to keep the crystal stationary, it was caught between two glass rods. One set of intensities was collected at room temperature by a θ–2θ scanning technique, to give 8053 unique reflections for $\sin\theta/\lambda \leq 0.703$ Å^{-1}. Within this set 4483 reflections were considered as observed according to the criterion $I > 3\sigma(I)$. Data were corrected for Lorentz-polarization and extinction effects. Corrections for crystal absorption were applied, but no improvement in the structure refinement was observed, probably due to the experimental conditions to keep the crystal stationary in the capillary. Atomic factors were taken from the "International Tables for X-Ray Crystallography" (11). All calculations were performed on a DEC microVAX 3100 computer with the *MolEN* software package (12).

Thermogravimetry and Differential Scanning Calorimetry

Simultaneous thermogravimetry (TG) and differential scanning calorimetry (DSC) measurements were carried out in a stream of nitrogen (40 ml min^{-1}) using a Thermoflex TG-DSC instrument (Rigaku) with a sample mass of about 15 mg. For TG measurements a sample mass of about 50 mg was spread evenly in a large sample holder to avoid mass effects and to reproduce as much as possible the experimental conditions used in TDXD. Air in the vessel was evacuated ($<10^{-2}$ Torr) before admitting the stream of nitrogen. TG analysis under vacuum was carried out using a thermobalance of McBain type with a sample mass of about 70 mg spread in a thin layer.

CRYSTAL STRUCTURE OF $Ag_2Ce(H_2O)(NO_3)_5$

Structure Determination

A monoclinic unit cell was found from powder pattern indexing. The parameters were used for reviewing the complete powder data by means of the evaluation program NBS*AIDS83 (13). The refined parameters were $a = 21.472(5)$, $b = 8.027(1)$, $c = 15.413(3)$ Å, $\beta = 90.45(2)°$, $V = 2656.5(7)$ Å^3 [$M_{20} = 32$, $F_{30} = 94(0.0058, 55)$]. (The powder data have been submitted to the ICDD (14) for possible inclusion in the Powder Diffraction File.) They are close to those reported for the related phases $Ce(NO_3)_5(H_3O)_2 \cdot H_2O$ [$a = 21.364(7)$, $b = 7.8990(7)$, $c = 15.133(2)$ Å, $\beta = 91.02(2)°$] (15) and $Na_2Nd(NO_3)_5 \cdot H_2O$ [$a = 21.216(9)$, $b = 7.903(4)$, $c = 15.147(5)$ Å, $\beta = 90.74(3)°$] (16), which suggests isostructural properties. In the present study, the systematic absences ($h0l$: $l = 2n + 1$) were in accordance with the space group $P2/c$. A three-dimensional Patterson function yielded the positions of three independent cerium atoms. From subsequent Fourier difference analyses all the remaining nonhydrogen atoms were found. The R and R_w factor values, based on the refinement of 435 parameters (thermal parameters were refined anisotropically) were 0.065 and 0.078, respectively. An attempt to locate hydrogen atoms failed. Crystal data and fractional atomic coordinates, with equivalent isotropic displacement parameters, are given in Tables 1 and 2. Selected bond distances and angles are listed in Table 3. Oxygen atoms of nitrate groups are noted O11 to O103; Ow1 and Ow2 correspond to water molecules.

TABLE 1
Crystal Data for $Ag_2Ce(H_2O)(NO_3)_5$

Crystal dimensions (mm)	$0.40 \times 0.20 \times 0.25$
Chemical formula	$Ag_2Ce(H_2O)(NO_3)_5$
Chemical formula weight (g mol^{-1})	683.89
Calculated density (g cm^{-3})	3.4194
Linear absorption (cm^{-1})	64.172
Crystal system	Monoclinic
Space group	$P2/c$
a (Å)	21.472(5)
b (Å)	8.027(1)
c (Å)	15.413(3)
β (°)	90.45(2)
V (Å^3)	2656.5(7)
Z	8
Radiation (Å)	0.71073
Data collection	h: $-21 \rightarrow 21$, k: $0 \rightarrow 11$, l: $0 \rightarrow 30$
Number of observations	4483
Number of variables	435
Weighting scheme	$\omega = 1/\sigma^2(F)$
R	0.065
R_w	0.078

TABLE 2
$Ag_2Ce(H_2O)(NO_3)_5$: Fractional Atomic Coordinates and Equivalent Displacement Parameters

Atom	x/a	y/b	z/c	B_{eq}
Ce1	0	0.1660(2)	0.25	1.56(2)
Ce2	0.24901(4)	0.1635(1)	0.25533(5)	1.56(1)
Ce3	0.5	0.1356(2)	0.25	1.56(2)
Ag1	0.11817(7)	0.2332(2)	−0.02484(8)	3.20(3)
Ag2	0.37153(6)	−0.1952(2)	0.03381(7)	2.96(3)
Ag3	0.12690(6)	−0.3476(2)	0.15652(8)	2.56(2)
Ag4	0.3933(1)	−0.3431(2)	0.3829(1)	5.06(4)
N1	0.0694(5)	−0.018(2)	0.1075(7)	2.1(3)
N2	0.3790(5)	0.339(2)	0.2825(7)	1.7(2)
N3	0.1248(5)	0.042(2)	0.3342(7)	1.7(2)
N4	0.2494(6)	−0.146(2)	0.1433(8)	2.3(3)
N5	0.4208(6)	−0.171(2)	0.2129(8)	2.2(2)
N6	0.5014(5)	−0.247(2)	−0.0604(8)	2.4(3)
N7	0.1840(6)	0.482(2)	0.3125(8)	2.2(3)
N8	0.3183(6)	0.023(2)	−0.1013(8)	2.3(3)
N9	0.0027(6)	0.471(2)	0.3677(8)	2.2(3)
N10	0.2464(6)	0.289(2)	0.0705(8)	2.6(3)
O11	0.0549(5)	−0.093(1)	0.1770(6)	2.3(2)
O12	0.0520(5)	0.130(1)	0.0986(7)	2.7(2)
O13	0.1003(6)	−0.087(2)	0.0519(7)	3.6(3)
O21	0.3755(5)	0.189(1)	0.2549(6)	2.1(2)
O22	0.3298(5)	0.412(1)	0.2985(7)	2.3(2)
O23	0.4305(5)	0.404(1)	0.2929(7)	2.2(2)
O31	0.0737(5)	−0.013(2)	0.3592(6)	2.6(2)
O32	0.1259(4)	0.147(1)	0.2716(6)	2.0(2)
O33	0.1739(5)	−0.001(1)	0.3681(6)	2.5(2)
O41	0.2042(5)	−0.113(1)	0.1944(6)	2.4(2)
O42	0.2939(5)	−0.044(1)	0.1427(6)	2.3(2)
O43	0.2490(6)	−0.270(2)	0.0973(8)	3.2(3)
O51	0.4397(5)	−0.131(1)	0.2895(6)	2.5(2)
O52	0.4344(5)	−0.062(1)	0.1549(6)	2.4(2)
O53	0.3904(6)	−0.301(1)	0.1985(7)	3.2(3)
O61	0.5427(5)	−0.294(2)	−0.1120(7)	3.0(2)
O62	0.4600(5)	−0.147(1)	−0.0887(7)	2.5(2)
O63	0.5000(6)	−0.295(2)	0.0151(7)	3.5(3)
O71	0.1966(5)	0.446(2)	0.2340(6)	2.6(2)
O72	0.2045(5)	0.380(1)	0.3689(6)	2.2(2)
O73	0.1553(5)	0.610(1)	0.3293(7)	2.7(2)
O81	0.3018(5)	−0.100(1)	0.3310(6)	2.3(2)
O82	0.3006(5)	0.128(1)	0.4070(6)	2.3(2)
O83	0.3494(5)	0.088(2)	−0.0450(7)	3.1(2)
O91	0.0439(5)	0.440(1)	0.1820(7)	2.6(2)
O92	0.0453(5)	0.360(1)	0.3683(7)	2.4(2)
O93	−0.0055(5)	0.597(2)	0.0879(8)	3.3(3)
O101	0.2016(5)	0.204(2)	0.1002(7)	2.8(2)
O102	0.2912(5)	0.319(2)	0.1211(7)	2.7(2)
O103	0.2465(6)	0.343(2)	−0.0031(7)	4.1(3)
Ow1	0.1258(5)	0.525(1)	0.0118(6)	2.6(2)
Ow2	0.3744(6)	−0.495(1)	0.0084(7)	3.0(2)

Note. $B_{eq} = (4/3) \sum_i \sum_j \beta_{ij}\, \mathbf{a}_i \cdot \mathbf{a}_j$ (Å^2).

Description of the Structure

The fractional atomic coordinates are similar to those reported for the structure of $Ce(NO_3)_5(H_3O)_2 \cdot H_2O$ (15), except for a translation $0, \frac{1}{2} - y, \frac{1}{2} - z$. The structure of the two compounds consists of isolated chains, formed by 12-fold-coordinated Ce polyhedra connected by nitrate groups running parallel to [100] (Fig. 1). Silver atoms and water molecules are located between the chains.

The cerium atoms are bonded to six bidentate nitrate groups in the form of an irregular icosahedron. The mean Ce–O distances (2.65(1), 2.64(1), and 2.64(1) Å for Ce1, Ce2, and Ce3, respectively) are in agreement with the value (2.65 Å) calculated by the bond-valence method (17, 18). The mean distance between two cerium atoms along the *a* axis is 9.660(1) Å. The Ag atoms are surrounded by nine O atoms as in the structure of the high temperature phase of $AgNO_3$ (19). The polyhedra are in the form of a distorted monocapped square antiprism for Ag1 (Fig. 2) and Ag2, which is less common than the tricapped trigonal prism generally described for a ninefold coordination. Ag4 is eightfold coordinated in the shape of a distorted square antiprism. Such a coordination number for silver has already been found in the structures of $Ag(ClO_4)(H_2O)$ (20) and $Ag_6Ce(NO_3)_9$ (21). For Ag3, the coordination is 8 + 1 and the polyhedron can be described by a square antiprism or a monocapped square antiprism. Indeed, the Ag3–O93 bond (3.06(1) Å) is greater than the other Ag–O distances (mean value 2.62(1) Å). Although such a distance is uncommon, the largest cation–anion distance that has been considered a bond is 3.15 Å for Ag–O according to Donnay and Allmann (22). Also, there are similar distances (3.02(5) Å) in the structure of the unstable phase of silver nitrate (23) and in $Ag_6Ce(NO_3)_9$ (3.09(2) Å) (21). The mean Ag–O distances (2.71(1) Å for Ag1, 2.66(1) Å for Ag2, and 2.67(1) Å for Ag3) are in good agreement with the value (2.65 Å) calculated by the bond-valence method (17, 18) for Ag bonded to 9 O atoms. The mean Ag4–O distance (2.65(1) Å) is shorter than those involving nine O atoms and is comparable to the value (2.61 Å) calculated for Ag bonded to 8 O atoms. It should be noted that the equivalent isotropic displacement parameter of Ag4 is high (5.06 Å^2). In fact, the thermal-motion probability ellipsoid was found to be very anisotropic in the [100] direction. This suggests a greater motion of Ag4 in a direction parallel to the chains of Ce icosahedra. It is worthwhile noting that the equivalent Na atom in the structure of $Na_2Nd(NO_3)_5 \cdot H_2O$ (16) has also been reported with a high equivalent isotropic displacement parameter (3.8 Å^2). The Ag polyhedra are sharing common vertices with four other polyhedra in the case of Ag1 and Ag4 and with five other polyhedra in the case of Ag2 and Ag3. Such connections form infinite zigzag chains in the three directions [100], [010], and [001], which describe a 3-dimensional network. In the *bc* plane, this canvas forms an irregular honeycomb generating tunnels along the *a* axis, which are filled by the chains of Ce icosahedra.

The 10 nitrate groups act as bidentate ligands. Two of them (N2, N3) bridge two icosahedra. Furthermore, these two nitrate groups ensure the connection between two

TABLE 3
$Ag_2Ce(H_2O)(NO_3)_5$: Selected Bond Distances (Å) and Angles (°)

			Within the Ce polyhedron				
Ce1–O11[i,ii]	2.65(1)	Ce2–O21	2.73(1)	Ce3–O21[i,iii]	2.71(1)		
Ce1–O12[i,ii]	2.61(1)	Ce2–O22	2.72(1)	Ce3–O23[i,iii]	2.70(1)		
Ce1–O31[i,ii]	2.71(1)	Ce2–O32	2.664(9)	Ce3–O51[i,iii]	2.58(1)		
Ce1–O32[i,ii]	2.728(9)	Ce2–O33	2.72(1)	Ce3–O52[i,iii]	2.57(1)		
Ce1–O91[i,ii]	2.61(1)	Ce2–O41	2.59(1)	Ce3–O61[iv,v]	2.64(1)		
Ce1–O92[i,ii]	2.58(1)	Ce2–O42	2.60(1)	Ce3–O62[iv,v]	2.64(1)		
		Ce2–O71	2.55(1)				
		Ce2–O72	2.65(1)				
		Ce2–O81	2.66(1)				
		Ce2–O82	2.59(1)				
		Ce2–O101	2.61(1)				
		Ce2–O102	2.59(1)				
			Within the Ag polyhedron				
Ag1–O12	2.52(1)	Ag2–O42	2.67(1)	Ag3–O11	2.59(1)	Ag4–O22	2.72(1)
Ag1–O13	2.85(1)	Ag2–O43	2.88(1)	Ag3–O13	2.70(1)	Ag4–O23	2.59(1)
Ag1–O31	2.69(1)	Ag2–O52	2.53(1)	Ag3–O41	2.58(1)	Ag4–O51	2.45(1)
Ag1–O33	2.77(1)	Ag2–O53	2.70(1)	Ag3–O43	2.86(1)	Ag4–O53	2.86(1)
Ag1–O73	2.70(1)	Ag2–O62	2.72(1)	Ag3–O71	2.53(1)	Ag4–O63	2.79(1)
Ag1–O93	2.94(1)	Ag2–O63	2.89(1)	Ag3–O73	2.75(1)	Ag4–O81	2.88(1)
Ag1–O101	2.63(1)	Ag2–O82	2.53(1)	Ag3–O91	2.50(1)	Ag4–O83	2.52(1)
Ag1–O103	2.91(1)	Ag2–O83	2.62(1)	Ag3–O93	3.06(1)	Ag4–Ow2	2.37(1)
Ag1–Ow1	2.42(1)	Ag2–Ow2	2.44(1)	Ag3–Ow1	2.45(1)		
Ag1–O13–Ag3	156.4(5)	Ag2–O53–Ag4	166.1(5)	Ag2–O43–Ag3	178.7(5)		
Ag1–O73–Ag3	133.0(4)	Ag2–O63–Ag4	139.6(4)				
Ag1–O93–Ag3	144.1(4)	Ag2–O83–Ag4	147.5(5)				
Ag1–Ow1–Ag3	128.1(4)	Ag2–Ow2–Ag4	132.7(5)				
			Within nitrate groups				
N1–O11	1.27(2)	O11–N1–O12	118(1)	N6–O61	1.25(2)	O61–N6–O62	118(1)
N1–O12	1.26(2)	O11–N1–O13	121(1)	N6–O62	1.28(2)	O61–N6–O63	122(1)
N1–O13	1.22(2)	O12–N1–O13	121(1)	N6–O63	1.23(2)	O62–N6–O63	120(1)
N2–O21	1.27(2)	O21–N2–O22	118(1)	N7–O71	1.27(2)	O71–N7–O72	115(1)
N2–O22	1.24(2)	O21–N2–O23	120(1)	N7–O72	1.27(2)	O71–N7–O73	120(1)
N2–O23	1.23(2)	O22–N2–O23	123(1)	N7–O73	1.22(2)	O72–N7–O73	124(1)
N3–O31	1.25(2)	O31–N3–O32	119(1)	N8–O81	1.26(2)	O81–N8–O82	118(1)
N3–O32	1.28(2)	O31–N3–O33	122(1)	N8–O82	1.27(2)	O81–N8–O83	122(1)
N3–O33	1.23(2)	O32–N3–O33	119(1)	N8–O83	1.21(2)	O82–N8–O83	120(1)
N4–O41	1.29(2)	O41–N4–O42	116(1)	N9–O91	1.28(2)	O91–N9–O92	115(1)
N4–O42	1.26(2)	O41–N4–O43	122(1)	N9–O92	1.28(2)	O91–N9–O93	122(1)
N4–O43	1.22(2)	O42–N4–O43	122(1)	N9–O93	1.22(2)	O92–N9–O93	123(1)
N5–O51	1.28(2)	O51–N5–O52	114(1)	N10–O101	1.27(2)	O101–N10–O102	117(1)
N5–O52	1.28(2)	O51–N5–O53	122(1)	N10–O102	1.26(2)	O101–N10–O103	123(1)
N5–O53	1.26(2)	O52–N5–O53	124(1)	N10–O103	1.21(2)	O102–N10–O103	120(1)
			Possible hydrogen bonds				
Ow1–O72	2.89(1)	O72–Ow1–O92	71.9(4)				
Ow1–O92	2.94(1)						
Ow2–O61	2.92(1)	O61–Ow2–O102	75.7(4)				
Ow2–O102	2.91(1)						

Symmetry codes. (i) x, y, z; (ii) $-x, y, \frac{1}{2}-z$; (iii) $1-x, y, \frac{1}{2}-z$; (iv) $1-x, -y, -z$; (v) $x, -y, \frac{1}{2}+z$.

icosahedra and a silver polyhedron $Ag4O_8$ and $Ag1O_9$ for N2 and N3, respectively. These nitrate groups (N2, N3) belong to the class III_{6b} proposed by Leclaire (24). The nitrate group N10 belongs to the class II_{3a} and bridges an icosahedron to a silver monocapped antiprism. All the remaining nitrate groups ensure the connections between an icosahedron and two silver polyhedra, generating the infinite chains of Ag polyhedra described before. They

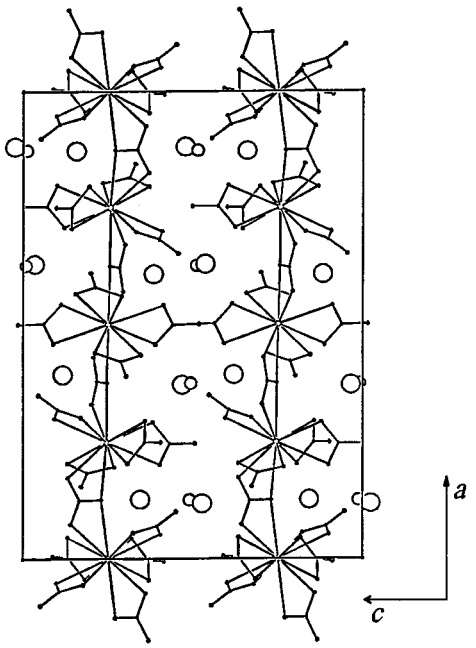

FIG 1. View of the unit cell of $Ag_2Ce(H_2O)(NO_3)_5$ along *b*, with *c* horizontal and *a* vertical. Large and intermediate sized circles correspond to Ag atoms and H_2O, respectively; small circles are Ce atoms surrounded by the nitrate groups.

belong to the class III_{6b} (N1, N4, N5, and N8) and to the class III_5 (N6, N7, and N9) reported by Leclaire (24). The water molecules, located between the chains of icosahedra, are bonded to the four silver atoms. Although attempts to locate hydrogen atoms failed, it has been possible to distinguish some hydrogen bonds (Table 3) according to Baur and Khan's criteria (25). These bonds bridge the Ce and the Ag polyhedra and the water molecules contribute significantly to the structural framework.

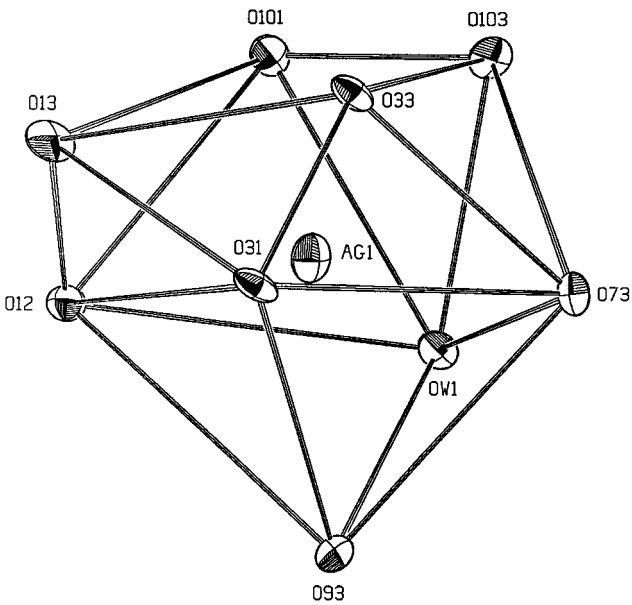

FIG 2. View of the environment of Ag1 atom, showing the distorted monocapped square antiprism consisting of eight O from nitrate groups and one water molecule (OW1). Displacement ellipsoids are plotted at the 20% probability level.

THERMAL DECOMPOSITION

The decomposition scheme of $Ag_2Ce(H_2O)(NO_3)_5$ carried out in flowing nitrogen (or air) was found to be different than that obtained in vacuum.

Thermal Decomposition in Nitrogen

The complex decomposition scheme of the precursor is pointed out by the different stages observed on the TG curve (Fig. 3, curve *a*) and on the TDXD plot (Fig. 4).

Dehydration of the precursor. From 80 to 115°C (Fig. 3, curve *a*), the water molecule evolves from the precursor (experimental weight loss: 2.60%, theoretical: 2.62%). However, from TDXD (Fig. 4) it is seen that the diffraction lines observed at 115°C disappear in two stages at higher temperature. This fact suggests that instead of the expected anhydrous compound a mixture of two phases is formed during the dehydration. To identify these phases, precise *in situ* powder diffraction data of the solid obtained at 140°C were collected. The position of several diffraction lines of the pattern were found close to those reported in the ICDD data base (45-0592) for cubic cerous potassium nitrate $K_3Ce_2(NO_3)_9$. From the indexing and the rewieving of the complete data set, a cubic solution with the cell parameter $a = 13.2648(8)$ Å $[M_{20} = 83, \quad F_{30} = 87(0.0093, 37)]$ was obtained. (The powder data have been submitted to the ICDD (14) for possible inclusion in the Powder Diffraction

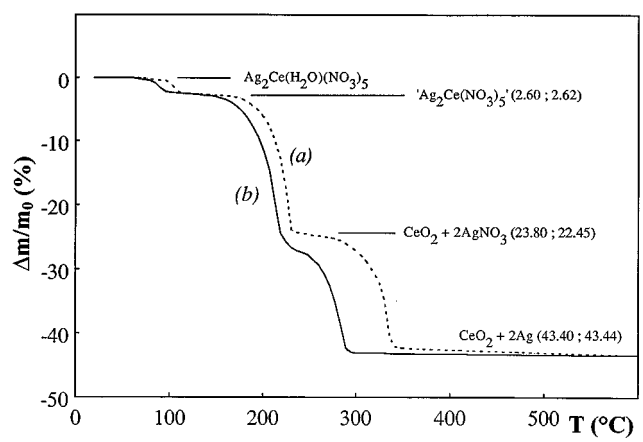

FIG 3. TG curves for the decomposition of $Ag_2Ce(H_2O)(NO_3)_5$ versus temperature. (*a*) in nitrogen; (*b*) under vacuum. Experimental and theoretical weight losses (%) are given in parentheses, respectively. Single quotes denote a chemical composition.

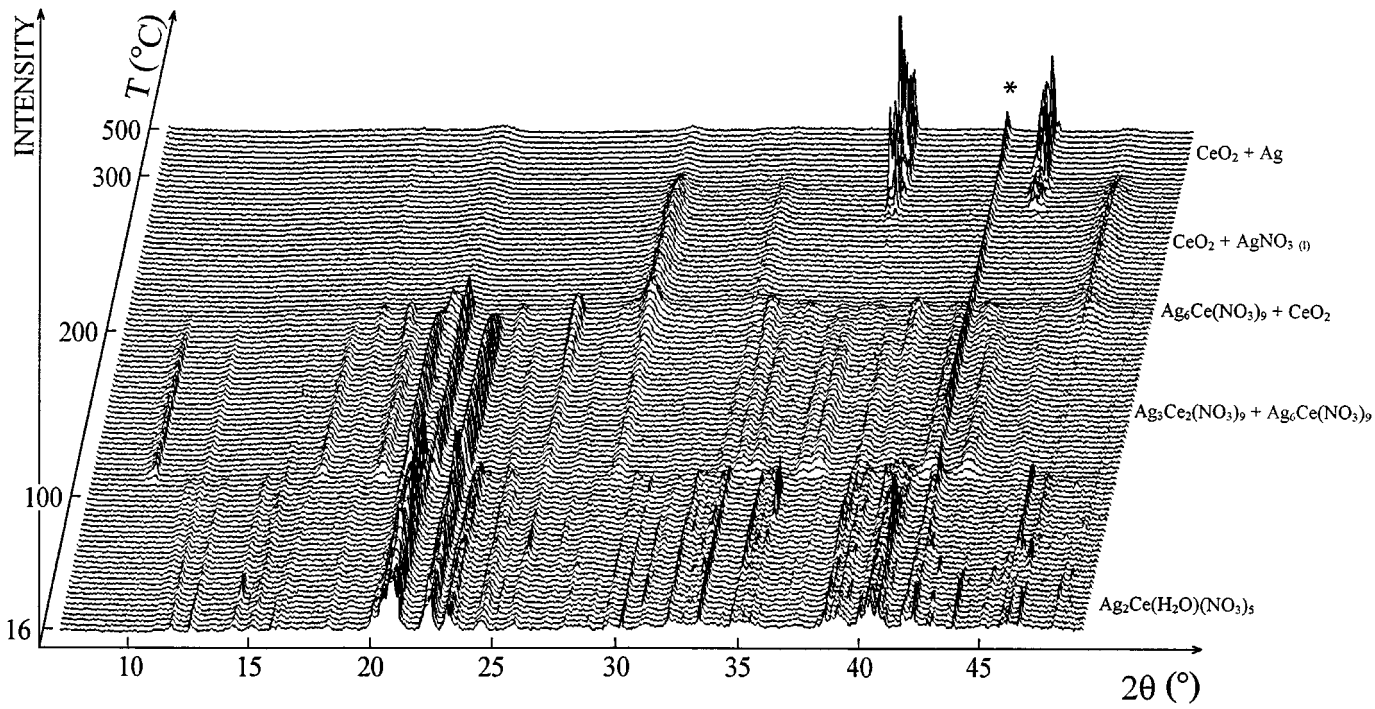

FIG 4. TDXD plot for $Ag_2Ce(H_2O)(NO_3)_5$ in nitrogen ($5°C\,h^{-1}$ in the range 16–300°C, $30°C\,h^{-1}$ in the range 300–500°C) with a counting time of 2500 s per pattern. * is a diffraction line of the sample holder.

File.) This solution compares well with that of the related compounds $Ln_2M_3(NO_3)_9$ (M = alkaline or ammonium ion, Ln = lanthanide) (4, 26–27). Consequently, $Ag_3Ce_2(NO_3)_9$ is one of the phases formed above 115°C. All the remaining lines of the diffraction pattern were found to belong to the pattern of $Ag_6Ce(NO_3)_9$ obtained independently in the course of this study and whose structure has been recently determined (21). Its diffraction pattern was indexed with a trigonal unit cell with the refined parameters $a = 16.467(3)$, $c = 14.646(4)$ Å, $V = 3440(1)$ Å^3 [$M_{20} = 29$, $F_{30} = 47(0.017, 38)$]. (The powder data have been submitted to the ICDD (14) for possible inclusion in the Powder Diffraction File.) From these results, the overall dehydration reaction can be written as:

$$9Ag_2Ce(H_2O)(NO_3)_5 \rightarrow 4Ag_3Ce_2(NO_3)_9 + Ag_6Ce(NO_3)_9 + 9H_2O. \quad [1]$$

The two phases decompose subsequently with different schemes in the temperature range 190–220°C (Fig. 4).

Decomposition of $Ag_3Ce_2(NO_3)_9$. The diffraction lines of $Ag_3Ce_2(NO_3)_9$ disappear before those of $Ag_6Ce(NO_3)_9$, while simultaneously the lines of CeO_2 emerge. The TG analysis reveals a weight loss (Fig. 3, curve *a*) until a plateau is reached at 230°C (experimental weight loss: 23.8%). To clarify this observation, a TDXD experiment was performed with a very slow heating rate of $1°C\,h^{-1}$ in the range 190–220°C (Fig. 5). The 3-D plot clearly shows that, in a first stage, the transformation of $Ag_3Ce_2(NO_3)_9$ yields not only CeO_2 but also an additional amount of $Ag_6Ce(NO_3)_9$, which in turn provides subsequently a new amount of CeO_2. This is better seen in Fig. 6 which shows the change of integrated intensity ratio I/I_{max} versus temperature for selected diffraction line of each phase (where I_{max} is a normalization factor corresponding to the maximum intensity for a given component). The absence of preferred orientation effects was controlled on a few lines of $Ag_6Ce(NO_3)_9$ and $Ag_3Ce_2(NO_3)_9$. At 140°C, I/I_{max} is 37.1% for $Ag_6Ce(NO_3)_9$. This result suggests that the total amounts of $Ag_6Ce(NO_3)_9$ obtained at 140 and 205°C (maximum of the intensity) respectively, are in the molar ratio 1 : 3. Consequently, the decomposition reaction of the four $Ag_3Ce_2(NO_3)_9$ molecules obtained in Eq. [1], can be written as

$$4Ag_3Ce_2(NO_3)_9 \rightarrow 2Ag_6Ce(NO_3)_9 + 6CeO_2 + 18(NO_2, NO, O_2). \quad [2]$$

From this hypothesis, the actual value of I/I_{max} can be calculated taking into account the X-ray absorption properties of the mixtures obtained at 140 and 205°C. Indeed, it is well known that the intensity of diffracted X-rays for a component is related to its mass fraction in the sample and to the mass absorption coefficient of the mixture (28). Based on

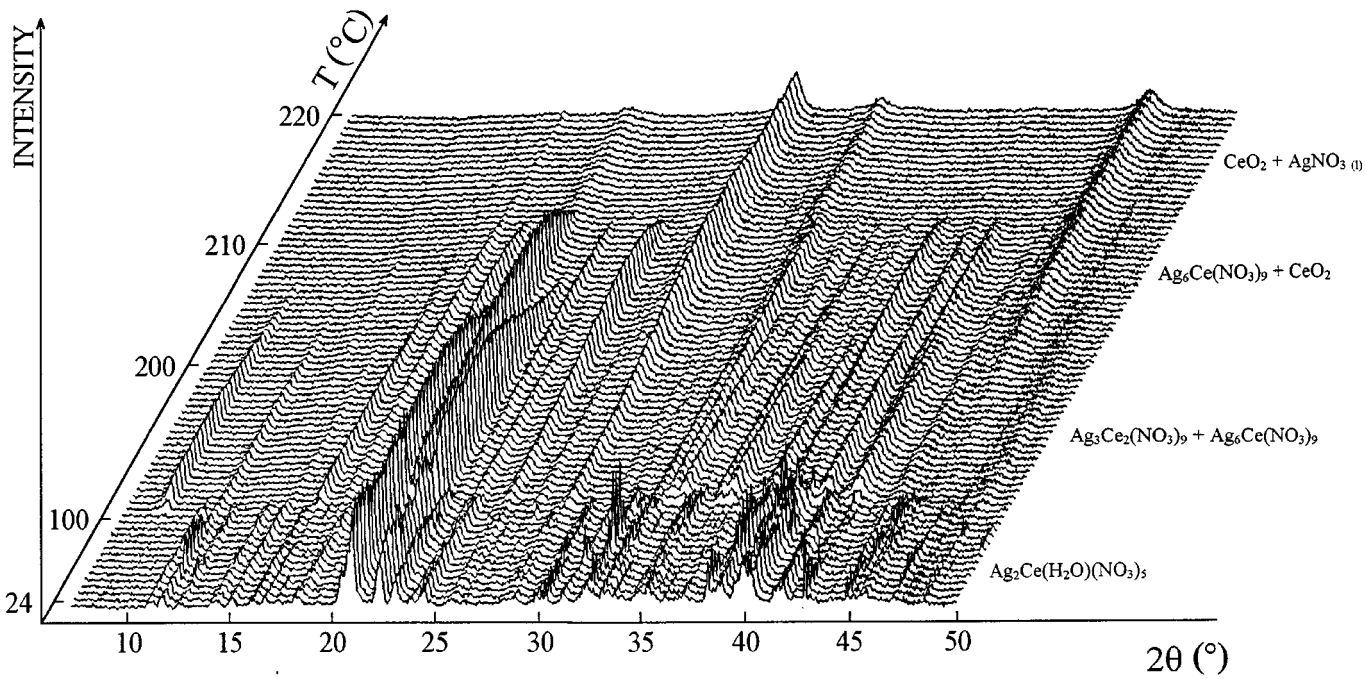

FIG 5. TDXD plot for $Ag_2Ce(H_2O)(NO_3)_5$ in nitrogen ($10°C\,h^{-1}$ in the range 24–190°C, $1°C\,h^{-1}$ in the range 190–220°C) with a counting time of 2000 s per pattern.

this property, phase abundance has already been derived for "dynamic" mixtures obtained in the course of thermal decompositions (29, 30). In the present study, if ω_1 and ω_2 denote the mass fraction of $Ag_6Ce(NO_3)_9$ in the mixtures (1) [$4Ag_3Ce_2(NO_3)_9$-$Ag_6Ce(NO_3)_9$] and (2) [$3Ag_6Ce(NO_3)_9$-$6CeO_2$] obtained at 140 and 205°C, respectively, we have at 140°C

$$I/I_{max} = (\omega_1/\omega_2) \times (\mu_2^*/\mu_1^*), \qquad [3]$$

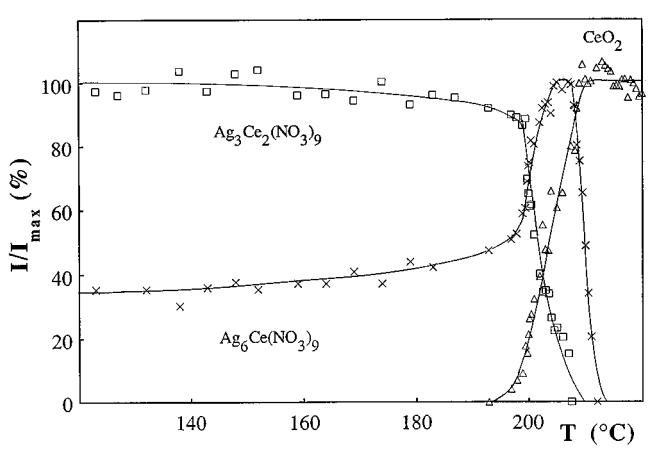

FIG 6. Integrated intensities of selected diffraction lines versus temperature from the TDXD plot in nitrogen for $Ag_2Ce(H_2O)(NO_3)_5$. □ line 221 of $Ag_3Ce_2(NO_3)_9$; × line 312 of $Ag_6Ce(NO_3)_9$; △ line 220 of CeO_2.

where μ_1^* and μ_2^* are the mass absorption coefficients of the two mixtures, calculated from the International Tables for Crystallography (31). From the assumption on the molar ratio 1 : 3 stated above, 0.225 and 0.700 were calculated for ω_1 and ω_2, respectively. Then, from Eq. [3], the ratio calculated for I/I_{max} is 37.5%, which is in good agreement with the experimental value 37.1%. Consequently, this calculation corroborates the stoichiometry of the proposed reaction scheme (Eq. [2]).

Decomposition of $Ag_6Ce(NO_3)_9$. Surprisingly, as shown by Figs. 5 and 6, only the intensities of the diffraction lines of CeO_2 increase during the subsequent decomposition of $Ag_6Ce(NO_3)_9$ in the range 205–215°C. On the other hand, the weight loss of 23.8% observed at 230°C (Fig. 3, curve *a*) compares well with the theoretical value (22.45%) calculated for the formation of a mixture of CeO_2 and $AgNO_3$ in the molar ratio 1 : 2. The formation of liquid $AgNO_3$ in this domain of temperature (melting point of $AgNO_3$: 209°C) would explain that only the diffraction lines of CeO_2 are observed in Figs. 4 and 5. This was supported by a DSC run which exhibited an exothermic peak at 210°C during the cooling of the phases obtained at 250°C. Consequently, the decomposition sequence of the three molecules of $Ag_6Ce(NO_3)_9$ formed in the two previous stages (Eqs. [1] and [2]) is

$$3Ag_6Ce(NO_3)_{9(s)} \rightarrow 3CeO_{2(s)} + 18AgNO_{3(l)} + 9(NO_2, NO, O_2)_{(g)}. \qquad [4]$$

Formation of metallic silver. Figure 4 shows that the diffraction lines of cubic silver emerge and increase in intensity from about 270 to 320°C. This is a complementary evidence of the formation of liquid silver nitrate in the precedent stage. Indeed, it is well known that the decomposition of $AgNO_3$ into Ag becomes appreciable 30–40°C above its melting point (32, 33). Accordingly, the end product of the decomposition of $Ag_2Ce(H_2O)(NO_3)_5$ is a mixture of CeO_2 and Ag. This conclusion is corroborated by the TG curve (Fig. 3, curve *a*) (final experimental weight loss: 43.4%, theoretical: 43.44%). Nevertheless, it can be observed that, in this last stage, the major part of the weight loss occurs after the formation of silver and is total only above 500°C. This may be due to difficulty to desorb the gaseous products from the solids.

In addition, the following features deserve to be mentioned:

i. The diffraction line broadening observed for CeO_2 and Ag above 320°C is quite different. Indeed, the diffraction lines of Ag are sharp (see Fig. 4) while those of CeO_2 are broad. This is an indication on the formation of large crystallites of Ag and nanoscale crystallites of CeO_2. This is supported by the SEM micrograph in Fig. 7 of a decomposition product obtained at 500°C. It shows large crystals of Ag whose faces are well defined with sizes of several μm. An average size of about 50 nm could be deduced for the CeO_2 grains, which are in fact composed of smaller diffracting domains, as revealed by diffraction line broadening.

ii. The intensity of the diffraction lines of CeO_2 decreases dramatically as the amount of Ag increases in the range 270–320°C (Fig. 4). This result is rather surprising since the amount of CeO_2 is constant during this process. The partial absorption of X-rays by the large crystals of Ag is a valuable explanation if they are preferentially located in the front surface of the sample. It can be thought that this covering occurs gradually during the growth of silver crystals from liquid silver nitrate.

iii. The line intensities of Ag display high fluctuations from one pattern to the other (Fig. 4). This is explained by critical changes of crystal orientation in the powder induced by varying thermal conditions and magnified by the use of a stationary sample in the diffraction optics.

Thermal Decomposition under Vacuum

The TG curve (Fig. 3, curve *b*) is similar to the curve obtained in nitrogen, except that the transformations take place at lower temperatures. However, the comparison of the 3-D plots obtained in nitrogen (Fig. 4) and in vacuum (Fig. 8) reveals that the decomposition scheme of the precursor is more complex in vacuum. The precursor dehydrates first, with the lost of the unique water molecule, into a new compound stable in the narrow temperature range 85–90°C. This fact was better demonstrated by a complementary TDXD experiment performed with a slow heating rate (2°C h^{-1}) between 85 and 140°C. A sample of

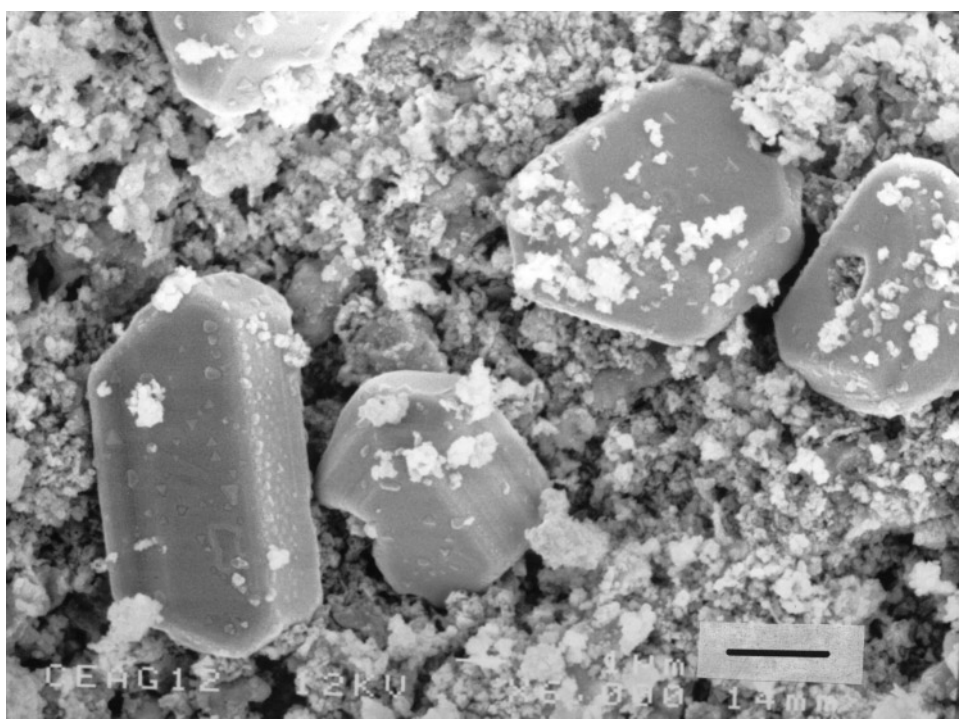

FIG 7. SEM micrographs (bar = 2 μm) of the mixture CeO_2–Ag obtained at 500°C from the decomposition under nitrogen of $Ag_2Ce(H_2O)(NO_3)_5$.

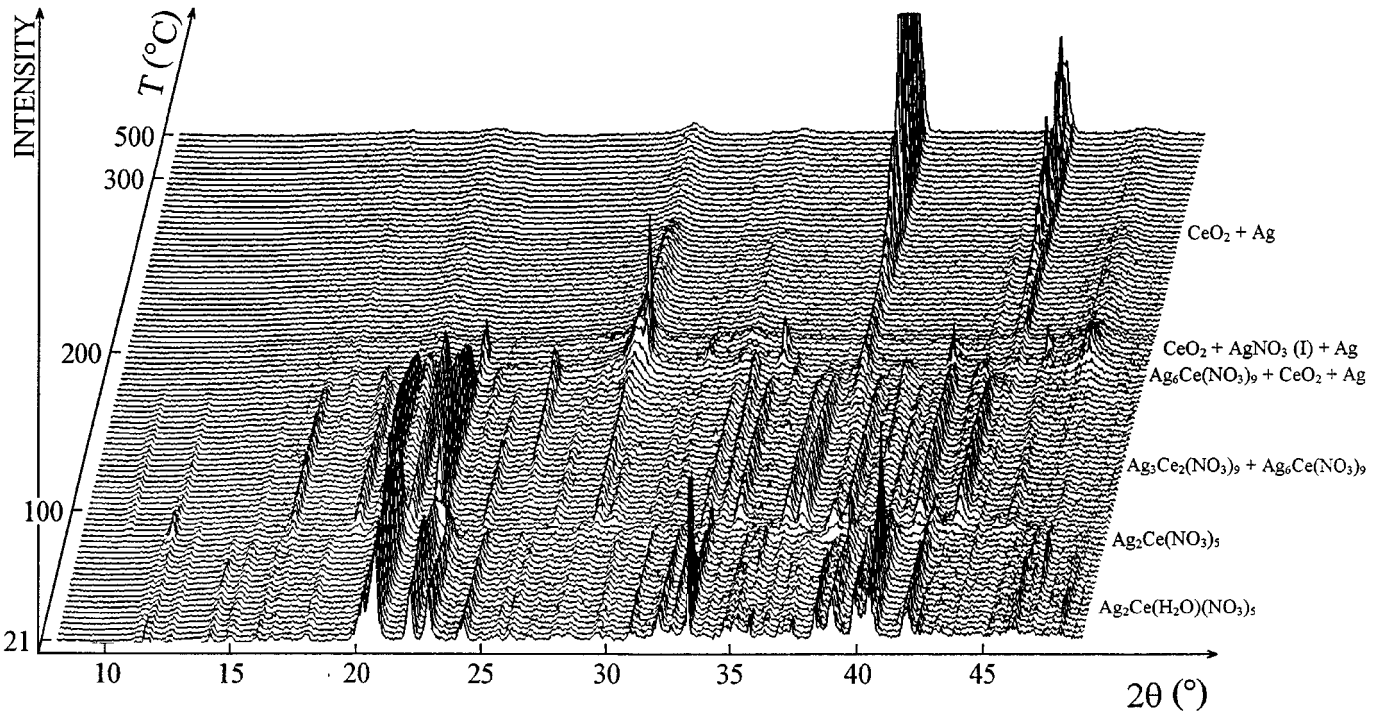

FIG 8. TDXD plot for $Ag_2Ce(H_2O)(NO_3)_5$ under vacuum (5°C h^{-1} in the range 21–300°C, 30°C h^{-1} in the range 300–500°C) with a counting time of 2500 s per pattern.

this phase could be obtained from the precursor heated at 85°C and then quenched at room temperature. From the indexing of its powder diffraction data, an orthorhombic unit cell with the following refined parameters $a = 10.258(3)$, $b = 10.799(3)$, $c = 11.567(3)$ Å, $V = 1281.3(4)$ Å^3 [$M_{20} = 18$, $F_{23} = 19(0.0102, 116)$] was obtained. The powder diffraction data of this compound are given in Table 4. As is often observed with decomposition products, it should be noted that the resolution of this pattern is low and, consequently, the precision of the indexing solution is moderate. However, the indexing demonstrates that the phase is pure and that the chemical formula is $Ag_2Ce(NO_3)_5$. The 3-D plots in Fig. 8 shows that this anhydrous phase transforms, above 90°C, into a mixture of $Ag_3Ce_2(NO_3)_9$ and $Ag_6Ce(NO_3)_9$ without weight loss (Fig. 3, curve *b*). Consequently, the two successive transformations can be written as

$$9Ag_2Ce(H_2O)(NO_3)_5 \rightarrow 9Ag_2Ce(NO_3)_5 + 9H_2O, \quad [5]$$

$$9Ag_2Ce(NO_3)_5 \rightarrow 4Ag_3Ce_2(NO_3)_9 + Ag_6Ce(NO_3)_9. \quad [6]$$

The thermal behavior of the mixture of the two phases is different from that observed in nitrogen. As depicted in Fig. 8, the transformation of $Ag_3Ce_2(NO_3)_9$ between 160 and 180°C provides not only CeO_2 and an additional amount of $Ag_6Ce(NO_3)_9$, but also cubic metallic silver, as

TABLE 4
X-Ray Powder Diffraction Data for $Ag_2Ce(NO_3)_5$

h k l	$2\theta_{obs}$ (°)	$2\theta_{calc}$ (°)	d_{obs} (Å)	I_{obs}
1 0 1	11.547	11.521	7.66	100
1 1 1	14.132	14.146	6.26	1
0 2 0	16.403	16.404	5.40	16
1 2 1	20.080	20.091	4.418	34
2 1 1	20.628	20.636	4.302	72
0 2 2	22.505	22.509	3.948	49
2 0 2	23.144	23.160	3.840	6
0 1 3	24.497	24.494	3.631	3
2 3 0	30.312	30.311	2.946	4
3 2 0	30.948	30.931	2.887	3
0 4 0	33.174	33.156	2.698	13
3 0 3	35.049	35.048	2.558	10
3 1 3	36.022	36.051	2.4913	3
2 3 3	38.414	38.420	2.3415	31
2 2 4	39.444	39.441	2.2827	1
2 4 2	40.847	40.835	2.2074	4
4 2 2	42.003	41.982	2.1493	4
1 5 0	42.754	42.750	2.1133	7
2 1 5	43.708	43.699	2.0693	13
3 2 4	44.287	44.284	2.0436	3
0 4 4	45.948	45.950	1.9735	12
4 0 4	47.356	47.341	1.1981	4
5 2 0		47.365		
0 5 3	48.240	48.258	1.8850	3

clearly revealed when zooming the plot in this temperature range. In the range 180–195°C, the subsequent decomposition of $Ag_6Ce(NO_3)_9$ yields trigonal silver nitrate (phase I) (34) and CeO_2. From these results, it is obvious that the stoichiometric coefficients in Eqs. [2] and [4] are no more valuable. Consequently, the weight loss observed at the end of this stage must be higher than the theoretical 22.45%. This is supported by the TG curve (Fig. 3, curve *b*) which shows that the weight loss is $\sim$26.5% for the inflection at 230°C where $AgNO_3$ is liquid. It is worth noting that a small amount of metallic silver is formed before silver nitrate. The further behavior of the mixture liquid $AgNO_3$–CeO_2 is similar to that observed in nitrogen atmosphere, i.e., ended by a mixture of nanoscale CeO_2 crystallites and large Ag crystals.

DISCUSSION AND CONCLUSION

$Ag_2Ce(H_2O)(NO_3)_5$ is the first member of the family of rare-earth pentanitrato complexes, $M^I_2Ce^{III}(NO_3)_5 \cdot H_2O$, formed with a monovalent transition metal. Among the monohydrate salts reported in the literature, it is structurally related to $Ce(NO_3)_5(H_3O)_2 \cdot H_2O$ (15) and $Na_2Nd(NO_3)_5 \cdot H_2O$ (16). The structure is described from chains of Ce polyhedra bridged by two nitrate groups and chains of AgO_8 and AgO_9 polyhedra.

The thermal decomposition scheme of the precursor is quite different from that reported for the related monohydrate alkaline compounds (35–40). In the previous studies, due to the high heating rate used in TG runs, the melting of the precursors occurs in a first stage and is followed by a complex decomposition which was not elucidated. On the contrary, by using a very low heating rate and the powerful TDXD technique associated with independent TG and DSC measurements, the decomposition process of $Ag_2Ce(H_2O)(NO_3)_5$ was completely described. It was found to be dependent on the environmental atmosphere. Furthermore, the indexing of powder patterns of all intermediate phases has contributed to their identification.

In a first stage, the departure of the water molecule from the solid yields $Ag_2Ce(NO_3)_5$ or a mixture of the two phases $Ag_3Ce_2(NO_3)_9$ and $Ag_6Ce(NO_3)_9$. The anhydrous phase is obtained only in vacuum and is stable in a narrow temperature range. Such anhydrous compounds arising from the dehydration of related hydrated alkaline salts were reported from TG studies, but they were not structurally characterized (37, 40–41). On the other hand, crystals of $K_2Er(NO_3)_5$ (42) and $Li_2M(NO_3)_5$ (M = La, Pr–Eu) (43) were obtained in molten alkaline nitrates and their structures were described. It was found that the cell parameters of $Ag_2Ce(NO_3)_5$ [$a = 10.258(3)$, $b = 10.799(3)$, $c = 11.567(3)$ Å, $V = 1281.3(4)$ Å^3] are comparable to those of $Li_2Pr(NO_3)_5$ [$a = 8.996(2)$, $b = 10.527(2)$, $c = 11.786(2)$ Å, $V = 1116.14$ Å^3, $Z = 4$, $Pnnm$]. This analogy suggests that these phases are likely isostructural. It can be noted that the parameters *a* and *b* of the Ag compound are greater, which is due to the ionic radius of the cation (Li^+: 0.60 Å, Ag^+: 1.28 Å for an eightfold coordination). Consequently, relationships between the structures of $Ag_2Ce(H_2O)(NO_3)_5$ and $Ag_2Ce(NO_3)_5$ can now be mentioned. Indeed, the infinite chains of Ce icosahedra parallel to [100] in the structure of the precursor are parallel to [010] in that of the anhydrous salt. Furthermore, the *a* axis of the precursor is twice the *b* axis of the anhydrous salt, which is in accordance with the ratio of cell volumes and the number of entities per unit cell. In the two structures, the Ag cations are located between the chains of Ce polyhedra and they are eightfold coordinated in the anhydrous compound, similarly to Ag4 cation in the precursor. Finally, the structural relationships between the two compounds clearly show that the skeleton of the structure is preserved during the departure of the water molecules. On the contrary, there are no structural relationships between the two last compounds and $Ag_6Ce(NO_3)_9$ and $Ag_3Ce_2(NO_3)_9$. It can only be noted that the structure of all the phases is built from irregular icosahedra in which Ce atoms are linked to six bidentate nitrate groups.

The power of TDXD has again been demonstrated in this study. The identification of all phases, often based on the use of powder pattern indexing, has greatly contributed to explain the complex solid state reaction schemes. The technique has been particularly useful when mixtures were formed without weight loss. Moreover, TDXD combined with DSC have pointed out that liquid and crystalline silver nitrate appeared during the decomposition. As for the nitrato complexes with the formulas $M^I_2Ce^{IV}(NO_3)_6$ (M^I = alkaline or ammonium ion) (1–4) and $M^I_2Ce^{III}(NO_3)_5 \cdot nH_2O$ (5–7) the intermediate single nitrate decomposes, i.e., into metallic silver in the present study. At last, the detailed knowledge of these mechanisms, leading at low temperature to nanoscale oxides should be of interest in the monitoring of the microstructural properties of catalysts.

ACKNOWLEDGMENTS

N. Audebrand is indebted to the Conseil Régional de Bretagne for financial support. We are indebted to Dr. P. Bénard-Rocherullé and Mr G. Marsolier for the collection of the single-crystal and powder diffraction data.

REFERENCES

1. N. Guillou, M. Louër, J. P. Auffrédic, and D. Louër, *Acta Crystallogr. C* **51,** 1029 (1995).
2. N. Guillou, J. P. Auffrédic, and D. Louër, *J. Solid State Chem.* **115,** 295 (1995).
3. N. Guillou, J. P. Auffrédic, and D. Louër, *J. Solid State Chem.* **122,** 59 (1996).
4. N. Audebrand, N. Guillou, J. P. Auffrédic, and D. Louër, *Thermochim. Acta* **286,** 83 (1996).

5. M. Leskelä and L. Niinistö, *in* "Handbook of the Physics and Chemistry of Rare Earths" (K. A. Gschneidner, Jr. and L. Eyring, Eds.), p. 302. Elsevier, Amsterdam, 1986.
6. N. Audebrand, J. P. Auffrédic, M. Louër, N. Guillou, and D. Louër, *Solid State Ionics* **84,** 323 (1996).
7. N. Audebrand, J. P. Auffrédic, and D. Louër, *Thermochim. Acta* (1997). [in press]
8. N. Guillou, J. P. Auffrédic, and D. Louër, *J. Solid State Chem.* **112,** 45 (1994).
9. A. Boultif and D. Louër, *J. Appl. Crystallogr.* **24,** 987 (1991).
10. J. Plévert, J. P. Auffrédic, M. Louër, and D. Louër, *J. Mater. Sci.* **24,** 1913 (1989).
11. International Tables for X-ray Crystallography, Vol. IV. Kynoch Press, Birmingham, 1974.
12. C. K. Fair, "MolEN. An Interactive Intelligent System for Crystal Structure Analysis." Enraf-Nonius, Delft, The Netherlands, 1990.
13. A. D. Mighell, C. R. Hubbard, and J. K. Stalick, "NBS*AIDS80," a Fortran program for crystallographic data evaluation, National Bureau of Standards, 1981. [U.S. Technical Note 1141] [NBS*AIDS83 is an expanded version of NBS*AIDS80]
14. International Centre for Diffraction Data, Newtown Square, PA.
15. N. Guillou, J. P. Auffrédic, M. Louër, and D. Louër, *J. Solid State Chem.* **106,** 295 (1993).
16. A. G. Vigdorchik, Y. A. Malinovskii, V. I. Adrianov, and A. G. Dryuchko, *Izv. Akad. Nauk. SSSR Neorg. Mater.* **26,** 2357 (1990).
17. I. D. Brown, *J. Appl. Crystallogr.* **29,** 479 (1996).
18. I. D. Brown, *in* "Structure and Bonding in Crystals" (M. O'Keeffe and A. Navrotsky, Eds.), Vol. II, pp. 1–30. Academic Press, 1981.
19. P. Meyer and J. J. Capponi, *Acta Crystallogr. B* **38,** 2543 (1982).
20. R. Wartchow and W. Ludwig, *Z. Kristallogr.* **210,** 879 (1995).
21. N. Audebrand, J. P. Auffrédic, P. Bénard-Rocherullé, and D. Louër, *Acta Crystallogr.* (1997). [in press]
22. G. Donnay and R. Allmann, *Am. Miner.* **55,** 1003 (1970).
23. P. Meyer, A. Rimsky, and R. Chevalier, *Acta Crystallogr. B* **32,** 1143 (1976).
24. A. Leclaire, *J. Solid State Chem.* **28,** 235 (1979).
25. W. H. Baur and A. A. Khan, *Acta Crystallogr. B* **26,** 1584 (1970).
26. W. T. Carnall, S. Siegel, J. R. Ferraro, B. Tani, and E. Gebert, *Inorg. Chem.* **12**(3), 560 (1973).
27. E. Manek and G. Meyer, *Z. Anorg. Allg. Chem.* **616,** 141 (1992).
28. L. E. Alexander and H. P. Klug, *Anal. Chem.* **20,** 886 (1948).
29. J. Plévert, thesis, University of Rennes, 1990.
30. M. Epple, *J. Thermal Anal.* **45,** 1265 (1995).
31. International Tables for X-ray Crystallography, Vol. III. Kynoch Press, Birmingham, 1974.
32. O. Knacke, O. Kubaschewski, and H. Hesselman, "Thermochemical Properties of Inorganic Substances," second ed. Springer-Verlag, Berlin, Heidelberg, 1991.
33. K. H. Stern, *J. Phys. Chem.* **1**(3), 1972.
34. C. N. R. Rao, B. Prakash, and N. Natarajan, "Crystals Structure Transformations in Inorganic Nitrites and Nitrates Carbonates," Pub. NBS-NSDRDS-53, p. 1. National Bureau of Standards, Washington, DC, 1975.
35. A. K. Molodkin, Z. K. Odinets, A. V. Chuvelev, T. N. Ivanova, and A. I. Ezhov, *Russ. J. Inorg. Chem.* **24**(9), 1332 (1979).
36. A. K. Molodkin, Z. K. Odinets, Y. A. Grigor'ev, and A. I. Ezhov, *Russ. J. Inorg. Chem.* **26**(9), 1286 (1981).
37. A. K. Molodkin, Z. K. Odinets, T. V. S'edina, T. N. Ivanova, and A. I. Ezhov, *Russ. J. Inorg. Chem.* **26**(9), 1289 (1981).
38. A. K. Molodkin, Z. K. Odinets, T. V. S'edina, and T. N. Ivanova, *Russ. J. Inorg. Chem.* **27**(12), 1736 (1982).
39. A. K. Molodkin, Z. K. Odinets, T. V. S'edina, and T. N. Ivanova, *Russ. J. Inorg. Chem.* **28**(1), 56 (1983).
40. Z. K. Odinets, E. M. Senyatkina, A K. Molodkin, and T. N. Ivanova, *Russ. J. Inorg. Chem.* **34**(5), 644 (1989).
41. G. Meyer, E. Manek, and A. Reller, *Z. Anorg. Allg. Chem.* **591,** 77 (1990).
42. E. G. Sherry, *J. Inorg. Nucl. Chem.* **40,** 257 (1978).
43. E. Manek and G. Meyer, *Z. Anorg. Allg. Chem.* **619,** 513 (1993).